Computers, Materials & Continua

Tech Science Press

https://doi.org/10.32604/cmc.2026.083128

ARTICLE

Numerical Modeling and Static Contact Analysis for a Bioinspired Rigid-Soft Fingertip

Jiafeng Liu[1,2], **Junhao He**[1], **Binbin Deng**[1], **Jie Sun**[1], **Chenyu Shi**[1,3], **Shunhang Liang**[1], **Zicong Zhou**[1,4], **Guangsheng Feng**[1] and **Jie Zhang**[1,*]

[1]School of Mechanics and Construction Engineering, Jinan University, Guangzhou, China
[2]Department of Engineering Mechanics, Tsinghua University, Beijing, China
[3]School of Aeronautics and Astronautics, Zhejiang University, Hangzhou, China
[4]CAS Key Laboratory of Mechanical Behavior and Design of Materials, University of Science and Technology of China, Hefei, China

*Corresponding Author: Jie Zhang. Email: jiezhang@jnu.edu.cn

Received: 30 March 2026; Accepted: 10 June 2026; Published: 23 July 2026

ABSTRACT: The ability to achieve sufficient grasping force while maintaining conformal contact with objects is highly attractive for bio-inspired flexible robotic hands and grippers. In this paper, a flexible robotic hand design is developed inspired by the human hand, where the fingers have an embedded rigid phalanx wrapped in soft silicone rubber materials. A rigid-soft numerical model is developed to investigate the static contact behavior of a fingertip with a rigid flat using finite element (FE) analysis. The Ogden constitutive model is adopted to characterize the hyper-elastic behavior of the silicone rubber material and its parameters are determined by uniaxial tensile and compression experiments. The FE numerical model is validated against experimental contact radius measurements, indicating that the classical Hertz contact theory becomes inadequate for large-deformation rigid-soft contact, and the presence of an internal rigid core has a great impact on the contact behavior. It is observed that when the normal force is small, the maximum stresses occur near the contact area. As the normal force increases, the location of the maximum stresses gradually migrates to the interface between the soft tissue and the rigid bone, indicating that the interfacial stress should be considered in the fingertip design. A parametric study is further conducted to systematically evaluate the effects of contact angle, friction coefficient, and rigid bone size on the contact force-deformation relationship and the resulting stress distribution along the rigid-soft interface. The simulations show that, within a certain parameter range, the contact angle and the friction coefficient slightly affect the interfacial stress distribution, while the structural size has a significant effect. The interfacial stresses exhibit a U-shaped dependence on the rigid bone size, with optimal stress minimization achieved at a bone-to-fingertip radius ratio between 3/8 and 1/2 for the present rigid flat contact configuration. These findings provide novel insights into the fingertip contact behavior and can further inspire the design of the flexible manipulators.

KEYWORDS: Soft fingertip; rigid-soft model; contact analysis; finite element analysis; experimental validation

1 Introduction

With the development of advanced materials and robotics technology, bioinspired manipulators/grippers have attracted widespread attention. Conventional rigid grippers can easily achieve high output force, stability, and control accuracy; however, their inherent high stiffness also severely limits their compliance and makes it more difficult for them to perform various soft interactions. The rigid-soft or soft-rigid coupling strategy, which combines rigid and soft materials/structures in a complementary manner, is a promising way to overcome these limitations and achieve a relatively high grasping performance [1–3]. It can combine the advantages of rigid and soft parts: the rigid parts provide stiffness and controllability, while the soft parts provide compliance and adaptability. An example is the rigid-soft manipulators inspired by the human hands and fingertips, where a soft fingertip or soft pad is attached to a traditional rigid gripper to achieve compliance and interaction capability, while the advantages of rigid grippers can also be well inherited. Some representative fingertip designs include: (1) hemi-spherical soft fingertips involving contact with flat [4–7] or curved surface [8–10]; and (2) rigid-soft fingertips featuring a soft layer over an internal rigid core, with research addressing soft pad patterns [11–14], soft layer thickness [15–18], and contact or grasping behavior [19–21]. The rigid-soft fingertip design is more similar to the human fingertip, where the external soft layer resembles the soft tissue and skin, and the internal rigid core reproduces the phalangeal bone.

As the soft part of the fingertip tends to undergo large deformations and exhibit nonlinear mechanical characteristics, the contact behavior of soft fingertips is more complicated [22]. Tatara [23] proved that the classical Hertz contact model is suitable only for linear materials, and that the soft fingertip contacts cannot be treated the same way as linear elastic contacts. Xydas et al. [24,25] derived a power-law theory reflecting the nonlinear contact behavior of the hemispherical soft fingers through experiments and finite element (FE) analysis, where the nonlinear contact is characterized by a force-radius relationship. Venkatesh Raja and Malayalamurthi [5] compared seven popular hyper-elastic nonlinear material models in the contact modeling and analysis of the hemispherical soft fingertip, and revealed that the Ogden and Neo-Hookean models are more suitable for representing the hyper-elastic material behavior. For the soft fingertip with an internal rigid core, i.e., the rigid-soft fingertip, Tiezzi et al. [15,19,26] tested fingertips with three differently sized cores and showed the impact of the thickness of the compliant layer using the power law model and exponential model. Raja and Malayalamurthi [17,18] also modelled soft fingertips with an inner rigid core using the FE method and conducted contact simulations with the Ogden model to investigate the influence of the rigid core in the soft hemispherical fingertip. It was found that the power-law theory proposed in [25] becomes invalid. Moreover, soft fingertips with an inner core are preferable to entirely soft ones, as they maintain a balanced relationship between the area of contact, conformal nature, and grasping stability. Further designs and optimizations for the soft layer with an internal rigid core have been conducted in [11–13] using the FE analyses and experimental tests, with the aim of achieving the desired compliance properties for soft contact that replicate those of human fingers. Although significant progress has been made in understanding the complex contact behavior of soft fingertips, existing knowledge remains insufficient for practical applications. Two main gaps are identified: (1) Most studies have focused on contact deformation under normal loads, while the effect of varying contact angles between the soft fingertip and the reference object has not been well considered, which is a more common case in practical applications. (2) Few investigations have focused on the stress distribution in the soft fingertips, particularly for the rigid-soft fingertips under different contact angles, friction coefficients, and soft layer thickness, which could be essential for the fingertip design based on the strength criterion. To address these gaps, this study aims to develop an experimentally validated FE model of a rigid-soft fingertip and to further investigate the influence of contact angle, friction coefficient, and structural dimensions on load capacity and stress distribution. Emphasis is placed on stress distribution from the perspective of strength criteria, and a potentially favorable structural design will be recommended based on the findings.

Specifically, this paper investigates the static contact behavior of a rigid-soft coupled fingertip intended for bioinspired manipulators. A corresponding FE model by the software Abaqus is developed for contact analysis, and its effectiveness and reliability are validated through contact experiments. The study further reveals the influence of different contact angles, friction coefficients, and structural sizes on the load capacity and stress distribution of the rigid-soft fingertip during flat contact. Based on the contact analysis, discussions and conclusions are provided to support the development of artificial flexible manipulators.

This study makes the following novel contributions: (1) Developing and experimentally validating a rigid-soft FE model of the fingertip; (2) Investigating the effects of contact angle, friction coefficient, and soft layer thickness on fingertip stress distribution in contact with a rigid flat surface; (3) Conducting a combined parametric study to evaluate how these factors jointly influence load capacity and stress concentration; (4) Identifying a potentially favorable structural size design (e.g., bone-to-fingertip radius ratio) for bioinspired manipulators.

2 A FE Model with Experimental Validation for the Rigid-Soft Fingertip Contact

The development of a reliable numerical model is essential for capturing the nonlinear deformation characteristics of the soft fingertip contact. This section first describes the structural design of the bioinspired rigid-soft fingertip. Then, a FE model with experimental validation is presented for analyzing the contact behavior of the fingertip.

2.1 A Bioinspired Rigid-Soft Fingertip for Manipulators with Soft Contact Capability

A human-hand-inspired rigid-soft fingertip design is shown in Fig. 1. The fingertip is composed of two parts: an internal rigid part, serving as the phalanx and bone, and an external soft part, serving as the finger skin and subcutaneous tissue. The rigid 'bone' is covered by soft 'tissues', where the rigid bones can provide sufficient grasping capacity and the soft tissues can touch objects smoothly, like an actual finger during grasping. Therefore, by controlling the movement of the bones as the usual rigid manipulators, the manipulator with soft tissues can adapt to complex objects similarly to human hands. The tip of the fingertip and the end of the bone are simplified as hemispheres, while the rest of the soft pad and the bone body of the fingertip are simplified as cylinders. The outer diameter is set to be R = 8.0 mm, which is inspired by an average male's index fingertip [27]. The material selection of the rigid bone can refer to the usual rigid grippers, and the steel material is considered in the present study. There could be many candidates for the soft tissues, see Ref. [22], and impact force attenuation, conformability, and repetitive strain dissipation should generally be considered. The silicone rubber is adopted in the present study as it possesses outstanding properties at low and high temperatures, thermal and oxidative stability. Besides, the silicone rubber is exceptionally pure and is also suitable for use in the food and medical industries. Furthermore, the soft part and the rigid part are ideally coupled together through adhesive connections with a binder [1]. To evaluate the soft contact behavior of the fingertip and the proper size ratio of rigid/soft parts, the contact behavior of the fingertip is further investigated through developing an FE-based model in the following. A representative fixed rigid flat plate is considered as a simplified object's surface. The radius of the bone and the contact angle are expressed as r and θ, respectively. A large r indicates a small thickness of the soft part, and θ means various contact geometries.

2.2 Material Model and Parameters

The material parameters of the steel for the rigid bone are Young's modulus of 210 GPa and Poisson's ratio of 0.3. The silicone rubber for the soft tissue shows a nonlinear material behavior in large deformation during the contact process. The hyper-elastic material model [28] is used for the silicone rubber, and the material constitutive parameters are determined by the standard uniaxial tensile and compressive tests, where the compressive test is equivalent to the biaxial tensile test if the material is incompressible. The Ogden hyper-elastic material model [29] is adopted, which is defined by a function of strain energy:

$$U = \sum_{i=1}^{N} \frac{2\mu_i}{\alpha_i^2} \left(\overline{\lambda}_1^{\alpha_i} + \overline{\lambda}_2^{\alpha_i} + \overline{\lambda}_3^{\alpha_i} - 3 \right) + \sum_{i=1}^{N} \frac{1}{D_i} (J-1)^{2i} \tag{1}$$

where $\overline{\lambda}_i$ are the deviatoric principal stretches $\overline{\lambda}_i = J^{-1/3}\lambda_i$; λ_i are the principal stretches; J is the relative volume ratio; the number of terms in the summation, N, determines the order of the Ogden model, e.g., first-order Ogden at $N = 1$; and μ_i, α_i and D_i are material parameters. For the incompressible material, $D_i = 0$, and the second term is vanished as $J = 1$. If no value is given for the material compressibility in the hyper-elastic model, a default set of $K_0/\mu_0 = 20$ corresponding to Poisson's ratio of 0.475 can be used for the silicone rubber in software Abaqus. It is often used to approximate incompressible behavior while keeping the model computationally stable. Then, the initial shear modulus μ_0 and bulk modulus K_0 for the Ogden form are given by

$$\mu_0 = \sum_{i=1}^{N} \mu_i, K_0 = \frac{2}{D_1} \tag{2}$$

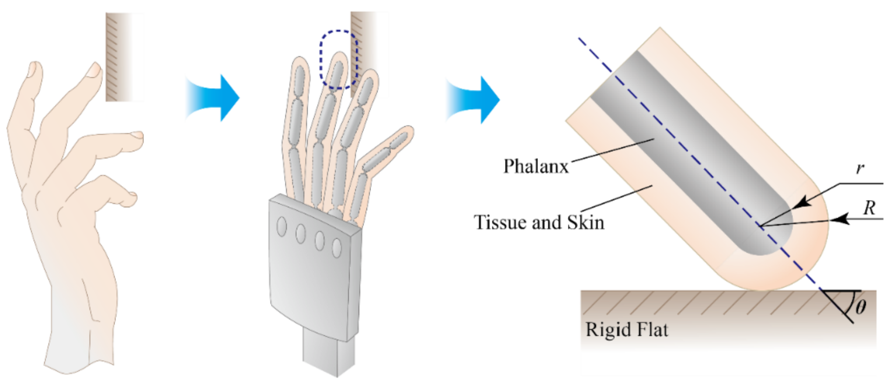

Figure 1: A bioinspired manipulator with rigid-soft fingertips and contacting the rigid flat surface.

Moreover, the viscosity is omitted as the simulation is considered quasi-static. Fig. 2 presents the uni-axial results of nominal stress vs. nominal strain, obtained from standard uniaxial tension and compression tests on typical specimens. The compression tests were conducted on cylindrical specimens (length 35 mm, radius 16 mm) at a loading speed of 5 mm/min. A loading speed of 50 mm/min was also tested for SampleC5, and the almost identical results indicate that the silicone rubber is rate-independent over the present loading rates (or strain rates). The tension tests were performed at 50 mm/min for greater testing efficiency. As the cross-sectional area of the tension sample outside the gauge length is nonuniform, the true strain rate is lower. The average results are obtained by first four specimens for each test condition. It is convenient that Abaqus can directly use the experimental data to define a hyper-elastic model for further simulation. Moreover, several typical hyper-elastic models can be explicitly fitted to the experimental data. Among them, the third-order Ogden model (Ogden_N3) shows better performance than lower-order Ogden models as well as other models such as the Neo-Hookean and Yeoh models. The parameters of the third-order Ogden model are presented in Table 1. Furthermore, FE simulations by software Abaqus with the C3D8RH element and the Ogden model for the uniaxial tension and compression specimens are performed, respectively. The results compared in Fig. 2c indicate that the FE model is sufficiently accurate, which guarantees the accuracy in simulating large deformation of the soft tissue of the fingertip.

Table 1: Hyper-elastic constants of the silicone rubber for soft tissue.

i	μ_i	α_i
1	−2.54312	1.22025
2	1.16605	1.51778
3	1.39944	0.92195

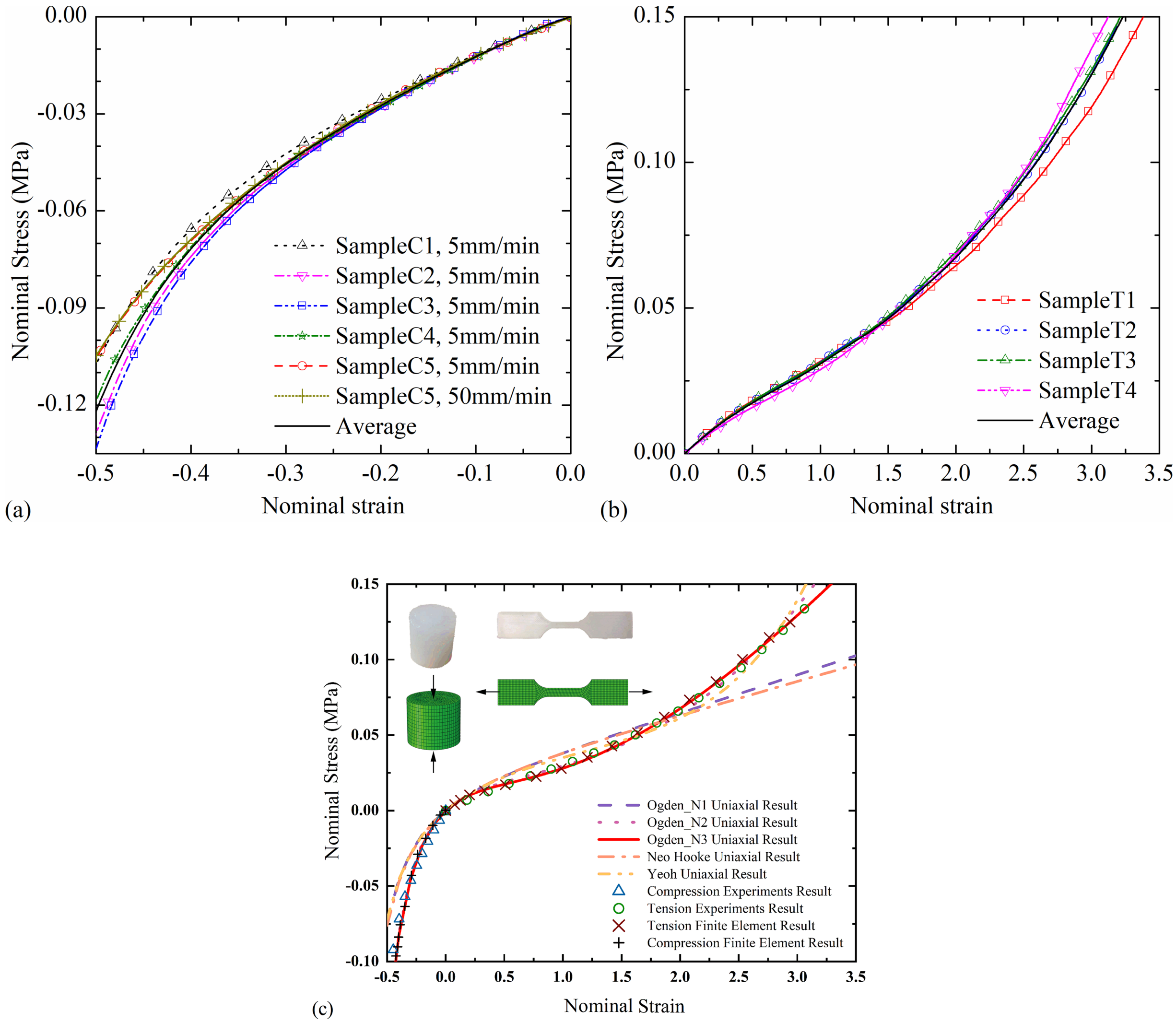

Figure 2: The uniaxial behavior of the silicone rubber: (**a**) The uniaxial compression tests; (**b**) The uniaxial tension tests; (**c**) The hyper-elastic material models based on the average uniaxial results.

2.3 Rigid-Soft Fingertip FE Modeling

The rigid-soft fingertip is further modeled by the FE software Abaqus to analyze the contact behavior. As the geometry, loading, and boundary conditions of the fingertip are symmetric, only half of the fingertip is modeled. The soft tissue is meshed by the C3D8RH element, which can simulate the nonlinear elastic behavior of hyper-elastic materials effectively, and the rigid bone is meshed by the C3D4 element, where a discrete rigid body model can also be used to improve simulation efficiency, as the bone undergoes negligible deformation. The mesh of the rigid bone is refined near the interface to match the mesh of soft tissue, and their interaction is set as a 'Tie' type in Abaqus. The interface between the fingertip and the flat is seeded with a fine mesh to provide enough resolution. Finally, a whole fingertip contact FE mesh model is illustrated in Fig. 3.

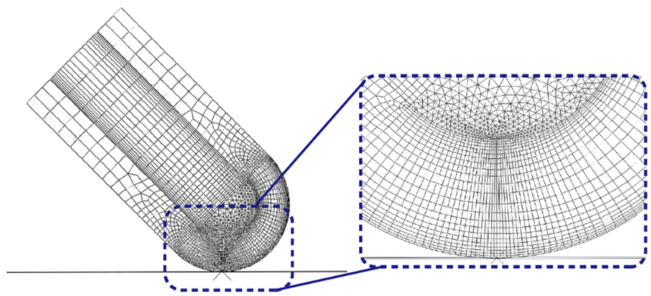

Figure 3: The rigid-soft fingertip FE modeling and meshing.

The static contact behavior is of great concern in this study. The boundary and load conditions for the simulation are as follows: (1) the rigid flat is fixed; (2) at the end opposite the fingertip's contact end, all translational and rotational motions of the rigid bone part are fixed except for displacement along the vertical axis; and (3) a concentrated vertical load is applied at the center of the rigid bone end. In software Abaqus, the normal and tangential behaviors between the fingertip and the rigid flat are defined as "Hard" contact and the "Penalty" friction formulation, respectively, with an initial friction coefficient of 0.3. The static solver is set to include the nonlinear effects of large displacements.

Through a convergence analysis with mesh refinement, the total number of elements in the adopted FE mesh ranges from approximately 55,000 to 120,000, depending on the soft tissue thickness. For the case of $r = 3.5$ mm and $\theta = 90°$ under a normal force of 1.0 N, Table 2 and Fig. 4 present the convergence results with mesh refinement. When approximately 55,000 elements are employed, the relative errors of the contact radius and the maximum Mises stress are both less than 1%.

Table 2: Contact solutions with various meshes for the case of $r = 3.5$ mm and $\theta = 90°$.

Total Number of Elements	Contact Radius (mm)	Maximum Mises Stress (kPa)
10,434	3.278	22.56
25,809	3.316	27.72
54,714	3.336	30.32
107,012	3.358	30.48

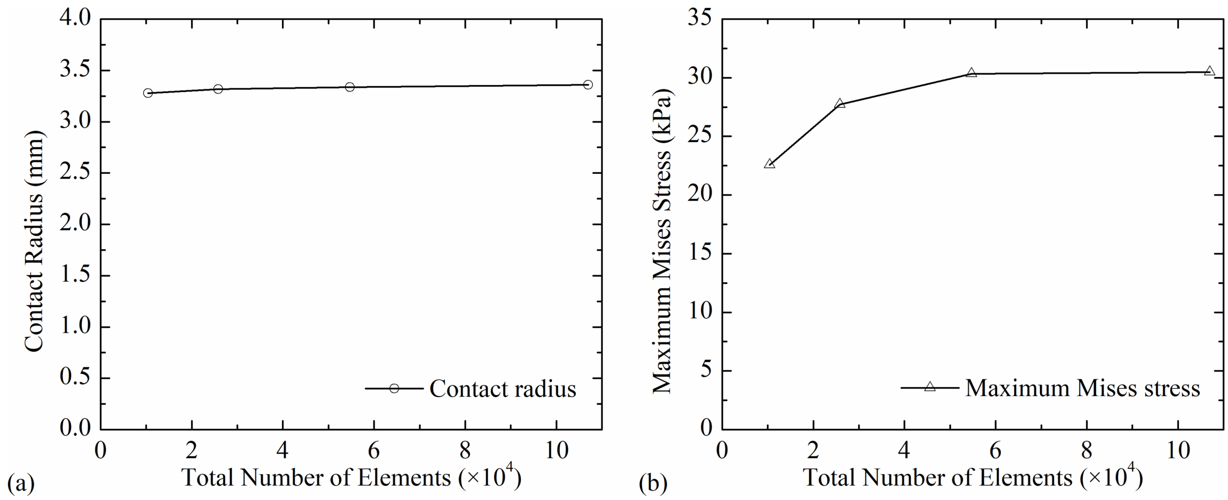

Figure 4: The convergent solutions with mesh refinement for the case of r = 3.5 mm and θ = 90° under a normal force of 1.0 N: (**a**) The contact radius; (**b**) The maximum Mises stress.

2.4 Validation of the Rigid-Soft Model for Static Contact Behavior

With a hemispherical tip on the present manipulator fingers, we use the Hertz contact theory to provide an approximate comparison for the soft contact behavior of the fingertip model. The typical Hertz contact theory is generally used to characterize the contact behavior of the linear elastic spheroids as shown in Fig. 5a. The growth of contact radius can be described as a function of the applied normal force as [30,31]:

$$R_{cH} = \left[\frac{3\pi R_1 R_2 F}{4\left(R_1 + R_2\right)} \left(\frac{1 - v_1^2}{E_1} + \frac{1 - v_2^2}{E_2} \right) \right]^{\frac{1}{3}} \tag{3}$$

where R_{cH} denotes the contact radius based on the Hertz theory, F is the normal force, R_i $(i = 1, 2)$ is the radius of two spheroids, v_i denotes Poisson's ratio, and E_i denotes Young's modulus.

In the present fingertip contact model, the radius and Young's modulus of one spheroid, i.e., the rigid flat, are infinity, see Fig. 5b, then Eq. (3) can be simplified as:

$$R_{cH} = \left[\frac{3\pi R_1}{4} \left(\frac{1 - v_1^2}{E_1} \right) F \right]^{\frac{1}{3}} \tag{4}$$

For the silicone rubber material used in the fingertip, E_1 and v_1 can be obtained from Eq. (2) and Table 1 (v_1 = 0.475 is considered).

Fig. 6 compares the contact radius (R_c) as a function of normal force for the fingertip according to Hertz theory, FE analysis and experiments. A pure soft fingertip model, i.e., without a rigid bone, and a rigid-soft fingertip with rigid bone r = 3.5 mm are selected. Hertz theory and FE analysis show a significant difference, as large and nonlinear deformation occurs during the soft contact process, and the assumptions of Hertz theory are not fully satisfied, which is consistent with the conclusion in [25]. Comparing the two FE analysis results, they indicate that the presence of rigid bone reduces the rate at which the radius of contact increases with normal force. In other words, when deformation exceeds a certain value, the behavior of the rigid-soft coupled fingertip cannot be simply described by Hertz theory or be simplified as a pure soft part, which is consistent with the findings in [17,18].

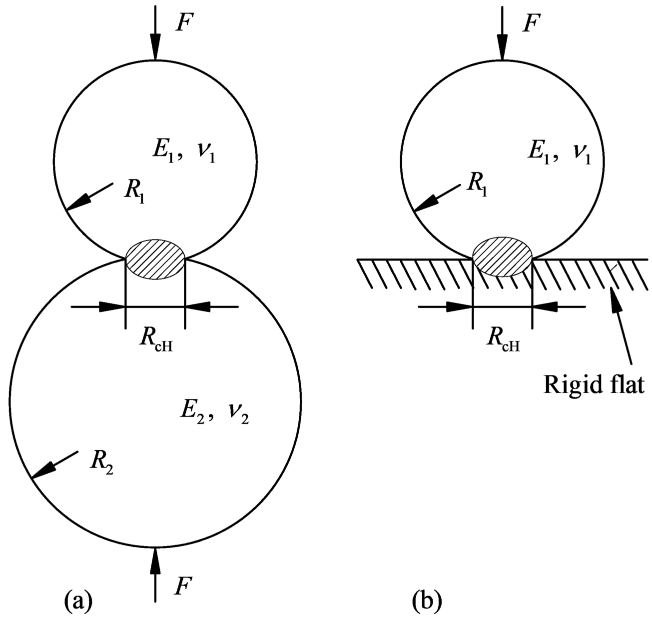

Figure 5: The Hertz contact model: (**a**) Contact between two spheres; (**b**) Sphere in contact with rigid flat.

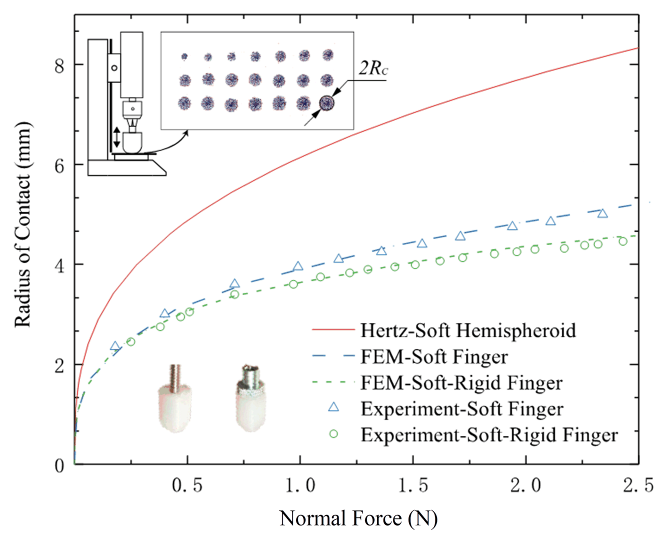

Figure 6: Comparison and validation of the FE model for rigid-soft fingertip contact.

The relationship between contact radius and normal force of the fingertip, considered a benchmark case, is experimentally investigated using a setup similar to that in Ref. [32], as shown in Fig. 6. The fingertip is mounted on a linear stage through a vertical pole and can be moved using the translation stage knob. When the fingertip contacts the platform surface, the normal force is displayed on an electronic force meter. The contact radius is measured directly from the fingertip imprint. The fingertip surface is coated with ink, which produces a clean, high-contrast imprint with a well-defined circumference on white paper, as illustrated in Fig. 6. The recording paper is placed on the platform surface and replaced for each applied normal force. The maximum force recorded on the force meter corresponds to the imprint obtained in each measurement. Although the applied normal force and the resulting deformation can be recorded and measured with good accuracy, they are difficult to precisely control at a specific target value in the present experiments. Nevertheless, each measurement can be regarded as an independent test, and the relationship can be reliably reproduced across varying applied normal forces and deformations. The experimental results show that the FE-predicted contact radii agree well with the measured values across the range of normal forces, thereby validating the effectiveness of the rigid-soft FE model in simulating the contact behavior between the rigid-soft fingertip and a rigid flat surface.

3 Rigid-Soft Fingertip Static Contact Results and Discussions

With the FE model validated against experimental results, this section presents a comprehensive analysis of the rigid-soft fingertip's contact behavior on a rigid flat. The influence of contact angle, friction coefficient, and rigid bone size on the load capacity and stress distribution is systematically investigated. Particular attention is given to the stress distribution from the perspective of strength criteria, as it is critical for the structural integrity of fingertip design.

3.1 Stress Distribution in the Rigid-Soft Fingertip during Static Contact

The stress distribution of the rigid-soft fingertip during the flat contact with rigid bone r = 3.5 mm is first investigated. Fig. 7 illustrates the fingertip deformation and the Mises stress distribution during the static contact process under a normal force of 1.0 N, a contact angle of 90°, and a friction coefficient of 0.3. The results for normal forces of 0.25, 0.50, and 0.75 N are also compared. When the normal force is small, the maximum Mises stress appears near the contact area. As the normal force increases, it can be found that the maximum Mises stress gradually shifts to the interface between the soft tissue and the rigid bone. Furthermore, when the applied normal force becomes large, which can still represent normal operational loads, the peak values of other stress components, such as normal and tangential stress, are also observed at the interface. This finding suggests that careful attention must be paid to the soft tissue strength and potential failure near the interface in fingertip design.

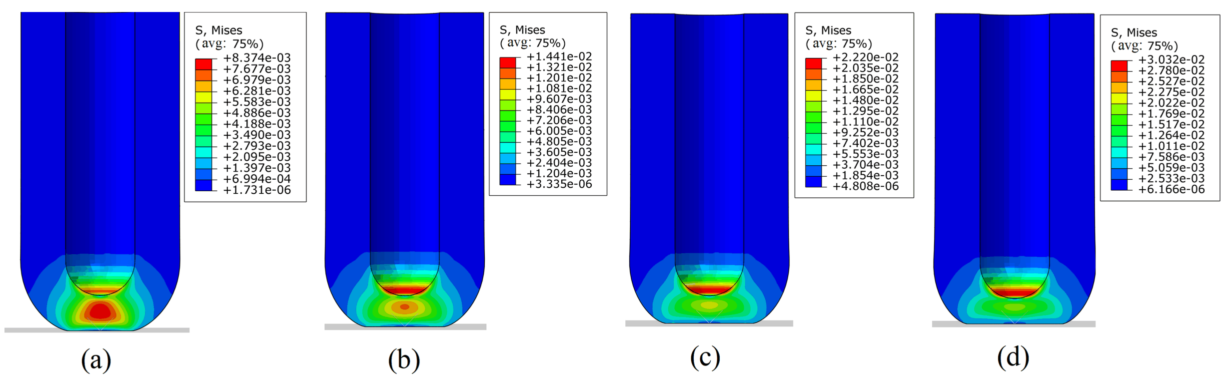

Figure 7: The Mises stress (MPa) distribution in the fingertip with various applied normal forces: (**a**) 0.25 N; (**b**) 0.50 N; (**c**) 0.75 N; (**d**) 1.0 N.

The interfacial stress distribution of the fingertip is further quantitatively illustrated in a spherical coordinate system, which is set in the center of the hemisphere as shown in Fig. 8a. Fig. 8b–d shows the distribution of the Mises stress, normal stress, and tangential stress under different contact angles with the same normal force of 1.0 N. The angular coordinate along the path is measured from the undeformed state, where the value "0°" is at the middle of the path, while "±90°" is at the edge of the path. It can be seen in Fig. 8b that, from 0° to 90°, the Mises stress first increases sharply, reaches the maximum values at approximately ±28°, and then decreases gradually. The distributions of the radial stress and the circumferential stresses, as Fig. 8c shows, yield a high concentration of stress at the middle of the path, which is relevant to the contact position. Although they have a similar distribution pattern, the magnitude of variation differs among them, and the peak of the Mises stress drifts laterally toward the sides. Fig. 8d illustrates the distributions of interfacial tangential stress. It can be found that the positive and negative peaks occur at the same point as the Mises stress peaks. In general, the interfacial stress distributions of the fingertip involve various factors. The peak values and distribution patterns vary across different stress components. Therefore, the comparison of different parameterized models is carried out in the following, where the interfacial Mises stress, radial stress, and tangential stress are considered as the main measures. It should be mentioned that the tangential stress is generally critical to the strength of the soft materials [33,34], and the interface tractions are essential for the interface strength, including debonding, slip, or delamination. Nevertheless, the current study does not address interface strength; instead, the soft-rigid interface is assumed perfectly coupled through an idealized adhesive binder.

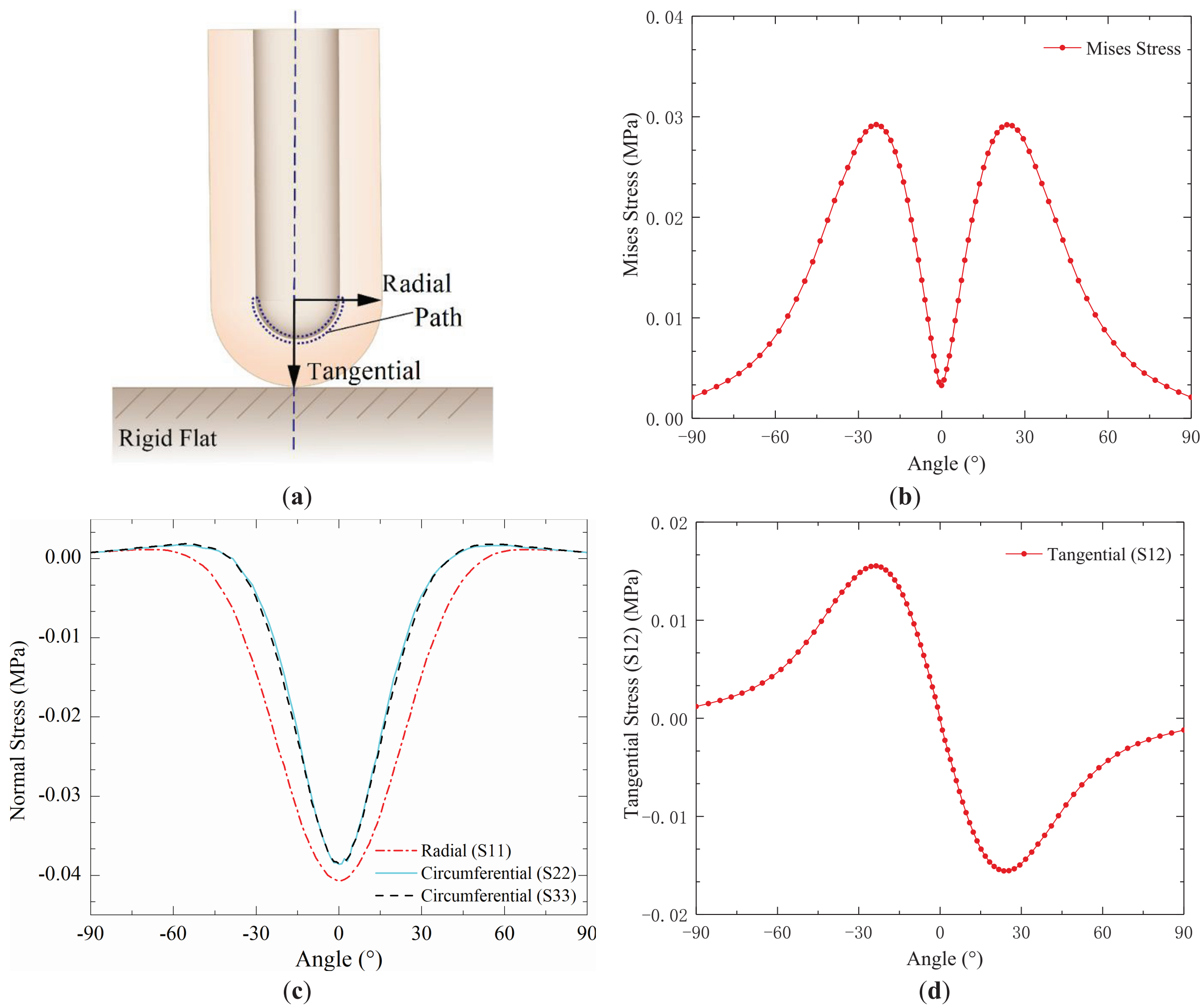

Figure 8: The interfacial stress distribution of the fingertip: (**a**) The contact configuration with a spherical coordinate system; (**b**) The Mises stress; (**c**) The normal stress; (**d**) The tangential stress (S12).

3.2 The Influence of Contact Angle

The contact behavior between the fingertip and the rigid flat in practice is more complicated than that under normal (straight-on) contact. Parameterized simulations of the fingertip with different contact angles are then conducted. The force-compression displacement curves for contact angles ranging from 10° to 90° are plotted in Fig. 9. The contact angle has only a slight influence on the force-deformation curves within a certain range, as the hemispherical fingertip exhibits similar deformation behavior when contacting the rigid flat at different contact angles. However, in the cases of 10° and 20°, the curves change significantly. This happens because the finger pad additionally engages in the contact, which considerably changes the contact area in large deformation. Nevertheless, it is beneficial to the fingertip contact as the load capacity is enhanced.

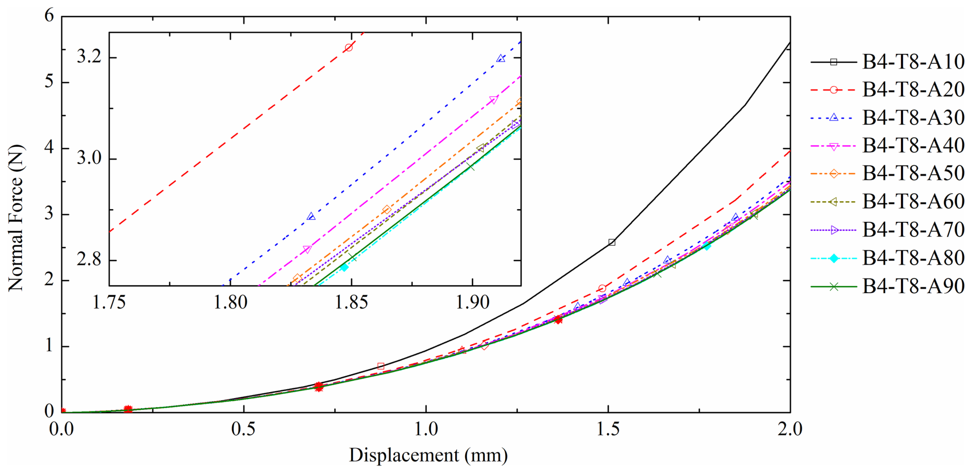

Figure 9: Force-vertical deformation relationship with various contact angles, where 'B' denotes the rigid bone radius, 'T' denotes the soft tissue radius, and 'A' denotes the contact angle.

A spherical coordinate system is also set at the center of the hemisphere as shown in Fig. 10a. Fig. 10b–d illustrates the interfacial stress distribution, including the Mises stress, radial stress, and tangential stress, of the fingertip under different contact angles at a constant normal force of 1.0 N. The stress distribution patterns are found to be similar across cases. For contact angles ranging from 30° to 90°, the stress distribution exhibits an approximate translational relationship with varying contact angle, which corresponds to a shift in the contact position. For the smaller angles of 10° and 20°, the stress distributions show some differences, such as the stress magnitudes being lower, which is beneficial to the load capacity of the fingertip as the finger pad also participates in the contact. Therefore, except for extremely small angles, the contact angle has only a slight influence on the stress distribution of a fingertip contacting a rigid flat. Consequently, it is reasonable to fix the contact angle in the fingertip model for subsequent studies, allowing the effects of other parameters to be investigated.

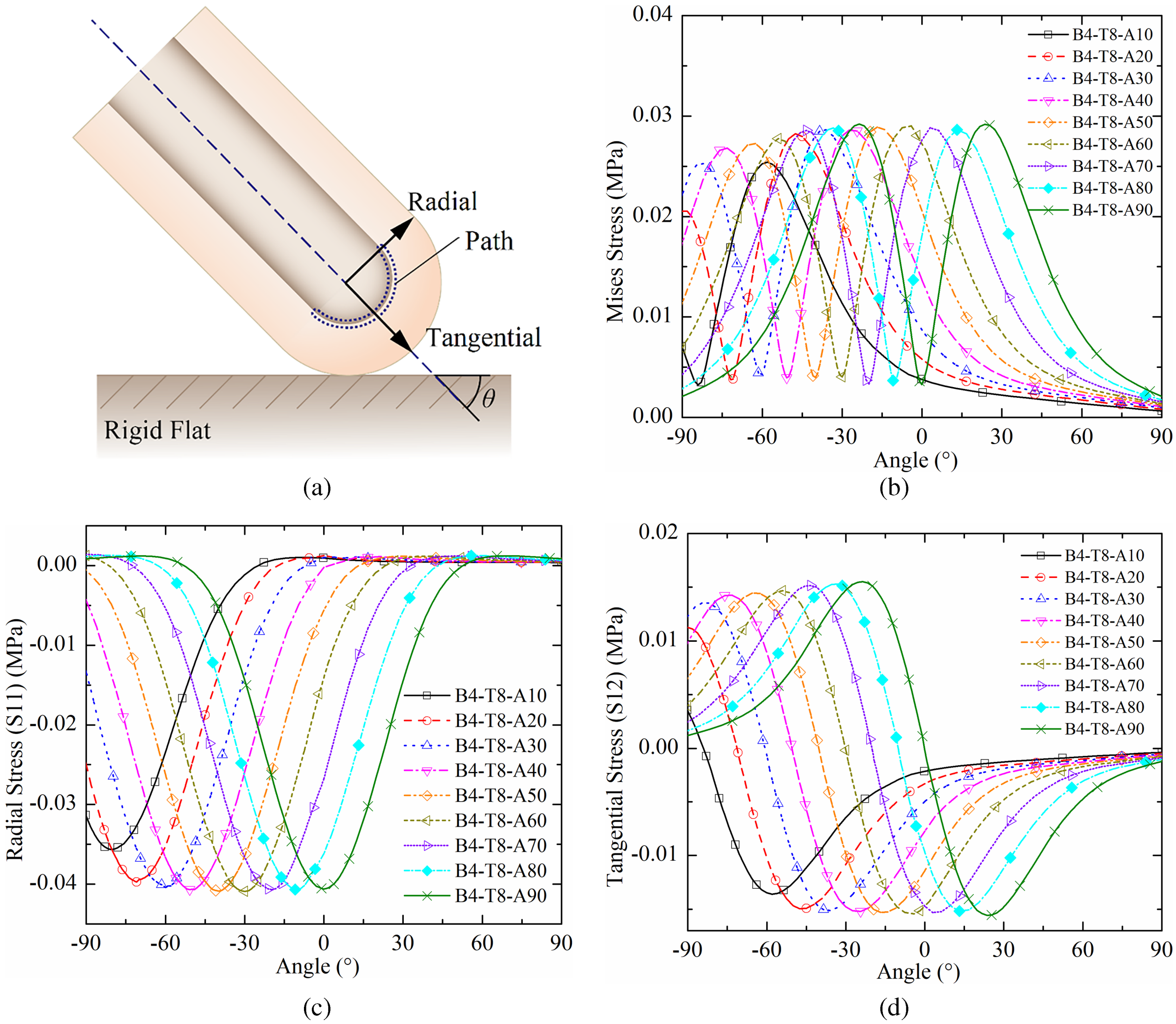

Figure 10: Interfacial stress distribution of the fingertip with various contact angles: (**a**) The contact configuration with a spherical coordinate system; (**b**) The Mises stress; (**c**) The radial stress (S11); (**d**) The tangential stress (S12).

3.3 The Influence of the Friction Coefficient

The friction coefficient between the fingertip and the rigid flat was set to 0.3 in the previous investigation. To better reflect practical conditions in which the manipulator could contact objects with various friction coefficients, a range of friction coefficients from 0.1 to 0.9 at a contact angle of 45° is further studied. The force-deformation response of the fingertip is shown in Fig. 11. It indicates that there is little difference in the force-displacement results across different friction coefficients when the deformation is small. However, apparent differences occur when the deformation exceeds about 1.2 mm. This is because the contact area between the soft finger and the rigid flat is initially small, making the frictional effect negligible. Under large deformation, a higher friction coefficient generates a larger tangential force that restrains the deformation of the soft tissue, thereby resulting in a smaller vertical displacement under the same force.

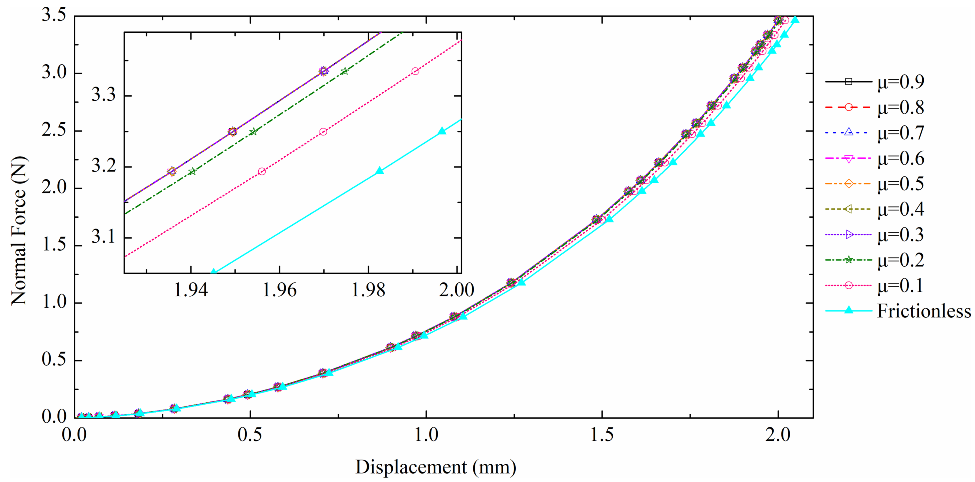

Figure 11: Force-vertical deformation relationship of fingertip with various friction coefficients.

Fig. 12 illustrates the interfacial stress distribution for different friction coefficients under the same normal force of 1.0 N. The results indicate that the stress distribution shows little difference when the friction coefficient is not less than 0.3, while the cases with small friction coefficients or the frictionless case exhibit considerably lower stress magnitudes, which are favorable for the strength of the fingertip. Nevertheless, only the static contact is considered in the present study. For different manipulator designs, it is necessary to select an appropriate friction coefficient based on the intended usage scenario, particularly when finger slipping is involved. Sometimes it is even necessary to increase friction by increasing the surface roughness of fingertips, for example, by adding epidermal ridges [35–37].

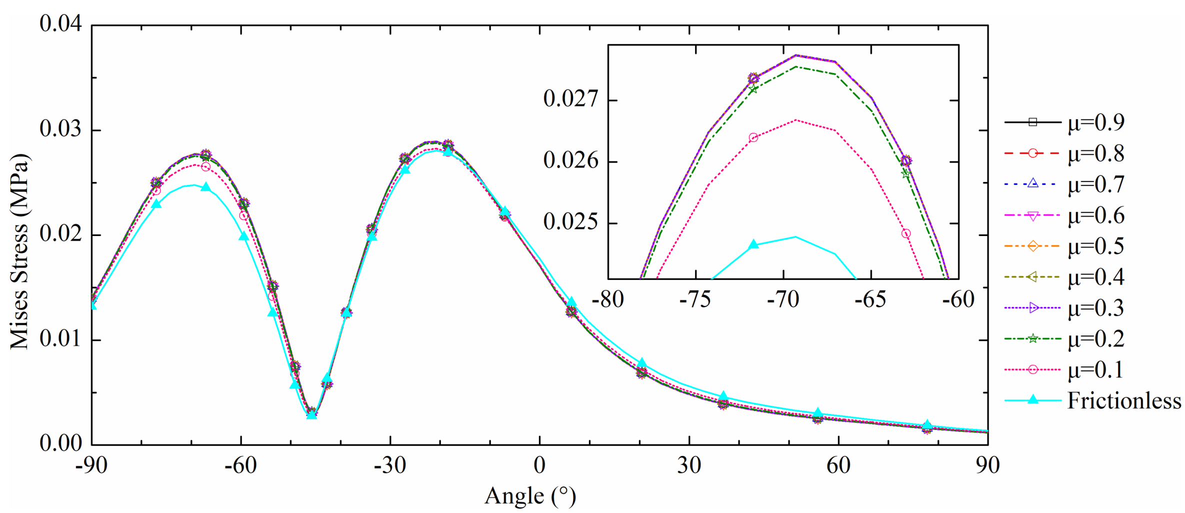

(a)

Figure 12: (Continued)

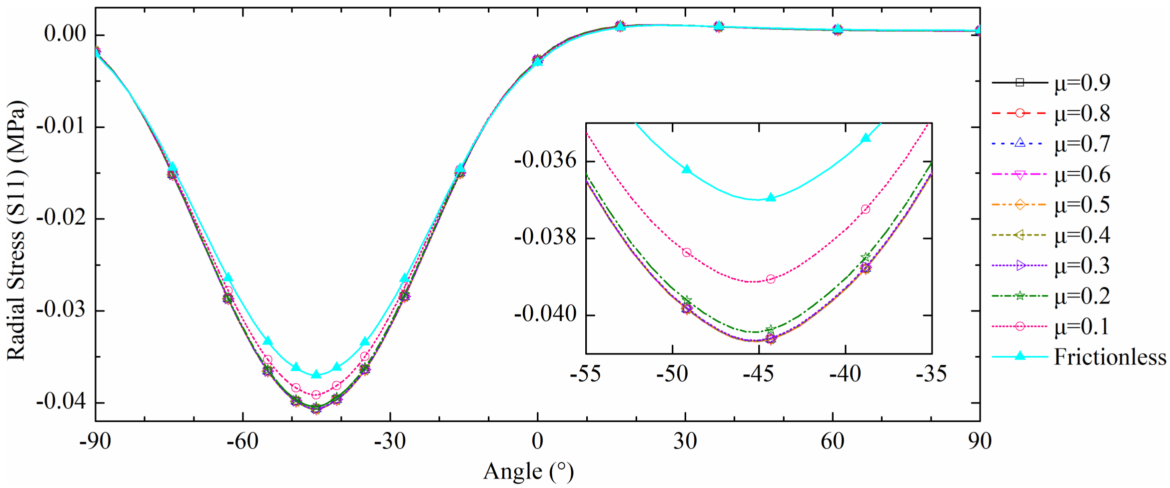

(b)

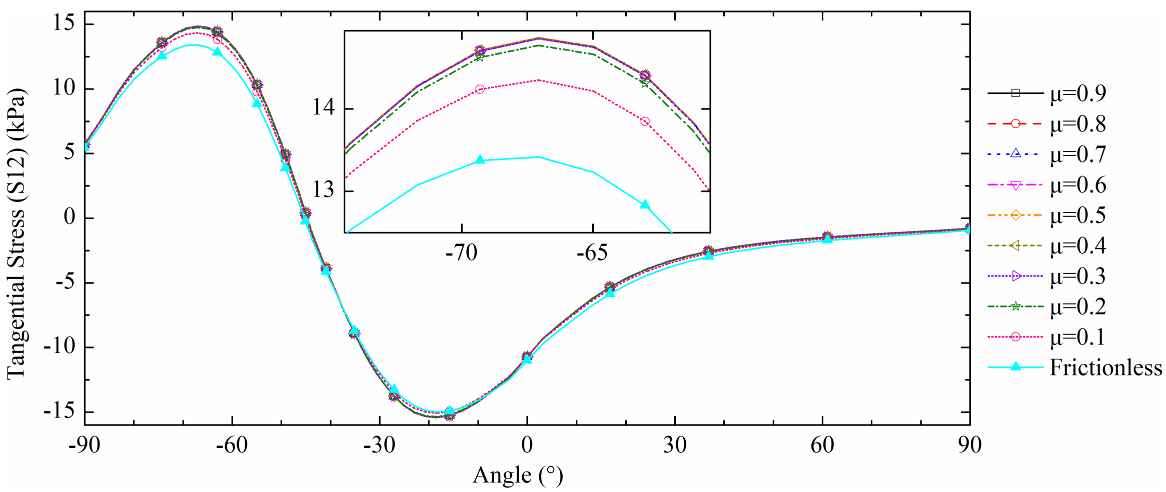

(c)

Figure 12: Interfacial stresses distribution of the fingertip with various friction coefficients: (**a**) The Mises stress; (**b**) The radial stress (S11); (**c**) The tangential stress (S12).

3.4 The Influence of the Rigid Component Size

A series of cases is conducted to investigate the influence of rigid bone size on fingertip contact with the rigid flat. The external radius of the fingertip model, i.e., that of the soft tissue, is fixed at 8 mm, while the internal bone radius ranges from 1.0 to 7.5 mm. Since variations in the contact angle (30° to 90°) and friction coefficient (above 0.3) have little influence on the interfacial stress distribution pattern under static contact with the rigid flat, a contact angle of 45° and a friction coefficient of 0.3 are selected as representative conditions for investigating the effect of rigid bone size.

Fig. 13 shows the force-vertical deformation relationship for various rigid bone sizes. Since the slope of the curve represents an equivalent stiffness of the fingertip, the equivalent stiffness increases with the rigid bone size. This is because the thickness of the deformable soft tissue on the fingertip decreases, resulting in less deformation or end displacement under the same load. When the bone-to-fingertip radius ratio (r/R) approaches 100%, the equivalent stiffness will tend to infinity, similar to that of rigid robot fingertips.

Conversely, when r/R is close to zero, the force-deformation curve becomes gentle, and the equivalent stiffness approaches that of fully soft robot fingertips.

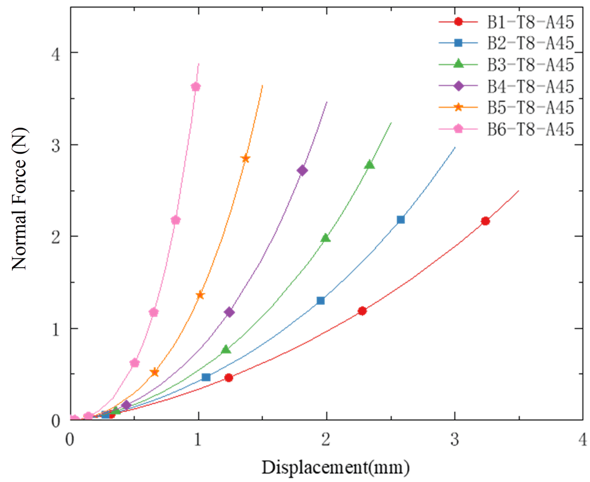

Figure 13: Force-vertical deformation relationship with various bone sizes.

Fig. 14 shows the interfacial stress distribution with different bone sizes under the same normal force of 1.0 N. The Mises stress distribution in Fig. 14a exhibits regular variations. As the bone radius increases from 1.0 to 4.0 mm, the peak stress continuously decreases, while the difference between the left and right peaks gradually diminishes. When the bone radius increases further from 4.0 to 7.5 mm, the peak stress increases, and the stress distribution becomes rapidly concentrated as the bone radius increases. The radial stress distribution in Fig. 14b also exhibits regular variations with the bone sizes. The peak radial stress occurs at −45°, which corresponds to the initial contact point and the center of the contact area. With increasing bone size, the stress distribution becomes increasingly concentrated. It can be inferred that when the bone size approaches the full fingertip, the stress distribution reverts to a rigid-like pattern. However, for small bone sizes (such as r = 1.0, 1.5, 2.0 mm), the maximum interfacial radial stress is higher than that for intermediate bone sizes. Moreover, distinct tensile stress appears at angles between 45° and 90°, corresponding to the back of the bone. This occurs because tissue deformation is so large that the tissue is extruded outward during fingertip compression, resulting in tensile stress on the back of the interface, which tends to cause outward deformation. This tensile stress effect also exists for larger bone sizes, but is often neglected due to its small magnitude. This finding suggests that when such a small bone size is adopted in the design of a bionic manipulator, it is necessary to evaluate the potential tensile stress that may cause interfacial debonding between the soft tissue and the bone.

The interfacial tangential stress distribution in Fig. 14c is similar to that of the interfacial radial stress, where the peak value first decreases and then increases as the bone size increases. The peak tangential stress occurs at −45°, which corresponds to the center of the contact area. In the case of small bones (such as r = 1.0 mm), the maximum interfacial tangential stress is found on the back of the bone and attenuates rapidly as bone size increases. This can be explained by the same mechanisms discussed for the radial stress. This finding indicates that when considering the use of such a bone structure in a bionic manipulator, attention should be paid to the possible occurrence of maximum tangential stress on the back of the bone, particularly for small bone sizes. Consequently, a more comprehensive verification of interfacial stresses is required to avoid interface slippage between the bone and the soft tissue.

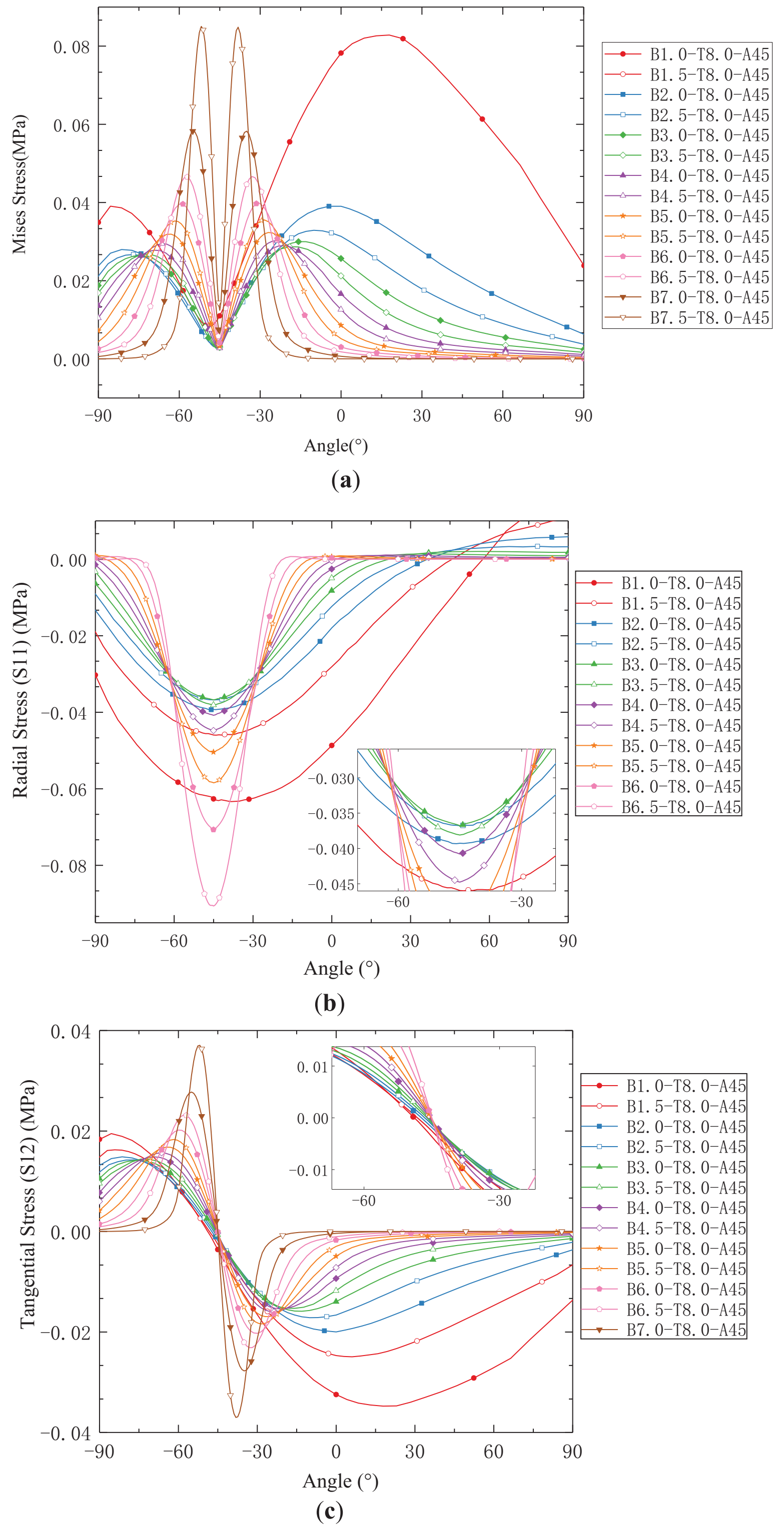

Figure 14: Interfacial stress distribution of the fingertip with various bone sizes: (**a**) The Mises stress; (**b**) The radial stress (S11); (**c**) The tangential stress (S12).

3.5 Bone-to-Fingertip Radius Ratio Design

As shown in the previous sections, the bone size, or equivalently the bone-to-fingertip radius ratio r/R, is the most influential parameter affecting both stiffness and interfacial stress distribution when the fingertip contacts a rigid flat surface. Two key observations are made: (1) the equivalent stiffness increases monotonically with r/R, ranging from that of a fully soft fingertip to that of a fully rigid one; and (2) the maximum interfacial stresses (Mises, radial, and tangential) could exhibit a U-shaped dependence on r/R. These observations indicate that an intermediate bone size minimizes the interfacial stresses.

The extreme values of the interfacial stress components are further presented and compared in Fig. 15. The maximum interfacial Mises stress first decreases and then increases with the bone size, exhibiting a U-shaped feature. When the bone size increases from 3.0 to 4.0 mm, the slope of the stress-bone size curve transitions from negative to positive, corresponding to the minimum interfacial Mises stress value. Similar features are also observed for radial stress and tangential stress, with their minimum values occurring in the range of 3.0 to 3.5 mm. This behavior can be attributed to the role of soft tissue as a pressure absorber in the rigid-soft coupled fingertip. Under the same applied pressure, a smaller bone results in a thicker soft tissue layer, which absorbs more pressure and thus reduces the pressure transmitted to the interface. However, a smaller bone also provides a smaller pressure-bearing area compared to a larger bone, which may lead to increased stress or non-negligible stress concentration. Consequently, both very large and very small bone sizes yield relatively high stress values. This trend is consistent with the anatomical design of human fingers, in which an optimal bone size exists. These findings are important for inspiring the design of robotic flexible manipulators. Therefore, based on the present investigation, a potentially favorable bone-to-fingertip radius ratio r/R from 3/8 to 1/2 is recommended within the present scope for the fingertip design, as it minimizes interfacial stresses when in contact with a rigid flat.

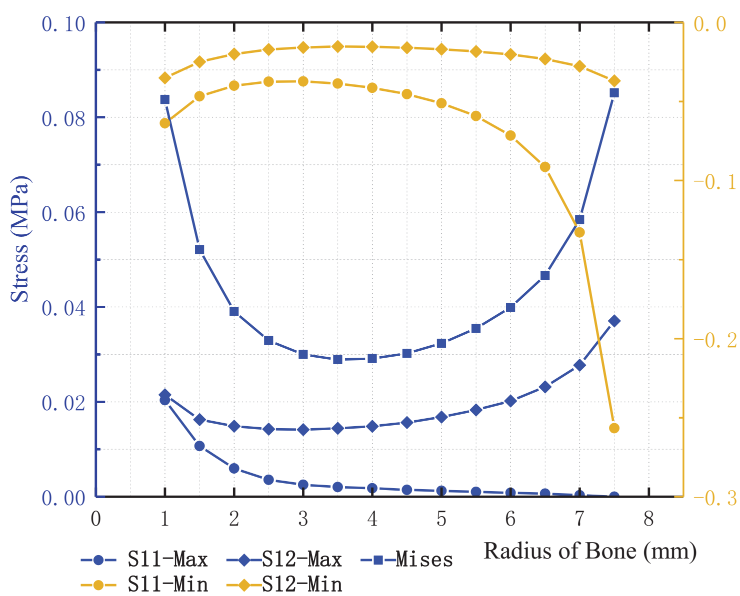

Figure 15: The extreme values of interfacial stress components with bone sizes.

This provides a useful baseline for bioinspired fingertip design within the scope of the present model assumptions (silicone rubber, rigid flat contact, quasi-static loading, and ideal bonding). Nevertheless, extrapolation to other materials, contact geometries, or loading modes, particularly for grasping curved or compliant objects, warrants caution and requires further validation.

4 Conclusions

This paper investigates the static contact behavior of a bioinspired rigid-soft coupled fingertip for flexible manipulator applications. The fingertip combines an internal rigid core with an external soft tissue, aiming to provide sufficient grasping capacity while enabling smooth object contact like the human hand. A rigid-soft finite element (FE) model capable of capturing large deformation and load-bearing capacity is developed to simulate static contact between the fingertip and a rigid flat surface representing a simplified object. The hyper-elastic behavior of the soft tissue is described using a third-order Ogden model. The FE model is validated against experimental measurements of applied force and contact radius using a fingertip fabricated from silicone rubber and steel. The results confirm that the contact behavior of the flexible manipulator cannot be adequately described by Hertzian theory, and that the presence of the internal rigid core significantly influences the contact response.

Using the validated model, a series of parametric studies is conducted to evaluate the effects of contact angle, friction coefficient, and rigid bone size on static contact behavior. As the normal force increases, the location of the maximum stresses migrates from the contact area to the soft tissue–rigid bone interface, indicating that interfacial strength is a critical concern in fingertip design. Accordingly, particular attention is paid to the force-deformation relationship and the resulting interfacial stress distribution.

The parametric study reveals the following key findings. First, under the present static contact conditions, variations in contact angle and friction coefficient have a slight influence on the fingertip contact behavior with the rigid flat surface, except when the contact angle or friction coefficient is very small. Notably, these exceptional cases are favorable for load capacity and fingertip strength. Second, the size of the internal rigid bone is the most influential parameter. The maximum interfacial stresses exhibit a U-shaped dependence on the rigid bone size, from which a potentially favorable bone-to-fingertip radius ratio that minimizes interfacial stresses can be identified. These findings provide a useful baseline for bioinspired fingertip design under the present model assumptions. Accordingly, for manipulator designs requiring a balance between compliance and interfacial durability under similar contact conditions, a bone-to-fingertip radius ratio of approximately 3/8 to 1/2 is recommended as a starting design guideline.

Several limitations of the present study should be acknowledged. The analysis is restricted to quasi-static loading and neglects the time-dependent viscoelastic behavior of silicone rubber, which may exhibit stress relaxation and hysteresis under cyclic or sustained loading. The contact scenario is simplified to a rigid flat surface, which does not fully represent real-world grasping tasks involving curved, textured, or compliant objects. The assumption of perfect bonding at the rigid-soft interface overlooks potential interfacial debonding or failure mechanisms under high-load or repeated loading conditions. Dynamic effects such as sliding, stick-slip behavior, and impact loading are not considered. Therefore, extrapolation of the present findings to other materials, contact geometries, or loading modes warrants caution and requires further validation, particularly for grasping curved or compliant objects, where additional analysis is recommended.

Future work will extend the current model to incorporate viscoelastic constitutive behavior and rate-dependent effects, enabling more realistic prediction of time-dependent responses. Investigations under dynamic and multi-axial loading conditions, including frictional sliding and grasping of irregular objects, will also be pursued. In addition, incorporating interfacial damage or cohesive zone modeling could provide a better understanding of failure mechanisms and long-term durability.

Acknowledgement: The authors would like to thank Guangdong Linzhi Technology Group Co., Ltd. for supporting the mechanical tests of the silicone rubber material.

Funding Statement: This research was funded by the National College Student Innovation Training Program of Jinan University (No. 202010559047), the Guangdong Undergraduate Innovative Research and Training Program of Jinan University (No. S202310559116, No. S202510559054), the Guangdong Basic and Applied Basic Research Foundation (2024A1515030048), and the Benchmark Course Development Project (2025QT075).

Author Contributions: The authors confirm contribution to the paper as follows: Conceptualization, Jiafeng Liu and Jie Zhang; methodology, Jiafeng Liu and Jie Zhang; validation, Junhao He, Binbin Deng, Zicong Zhou and Guangsheng Feng; investigation, Jiafeng Liu, Junhao He, Binbin Deng, Jie Sun, Chenyu Shi, Shunhang Liang, Zicong Zhou and Guangsheng Feng; writing—original draft preparation, Jiafeng Liu and Jie Sun; writing—review and editing, Jiafeng Liu, Junhao He and Jie Zhang; visualization, Jiafeng Liu; supervision, Jie Zhang; project administration, Jie Zhang; funding acquisition, Junhao He, Jie Sun, Zicong Zhou and Jie Zhang. All authors reviewed and approved the final version of the manuscript.

Availability of Data and Materials: The data that support the findings of this study are available from the Corresponding Author, Jie Zhang, upon reasonable request.

Ethics Approval: Not applicable.

Conflicts of Interest: The authors declare no conflicts of interest.

References

1. Chen H, Zhu J, Cao Y, Xia Z, Chai Z, Ding H, et al. Soft-rigid coupling grippers: collaboration strategies and integrated fabrication methods. Sci China Technol Sci. 2023;66(11):3051–69. doi:10.1007/s11431-023-2382-x.
2. He Z, Lian B, Song Y. Rigid-soft coupled robotic gripper for adaptable grasping. J Bionic Eng. 2023;20(6):2601–18. doi:10.1007/s42235-023-00405-2.
3. Li L, Crosby D, Shuttleworth M, Argin OF, Chen AS, Herrmann G, et al. A comparative analysis and scoping review of soft–rigid and industrial parallel rigid grippers. Adv Intell Syst. 2025;7(5):2400503. doi:10.1002/aisy.202400503.
4. Tiezzi P, Kao I. Modeling of viscoelastic contacts and evolution of limit surface for robotic contact interface. IEEE Trans Robot. 2007;23(2):206–17. doi:10.1109/TRO.2006.889494.
5. Venkatesh Raja K, Malayalamurthi R. Assessment on assorted hyper-elastic material models applied for large deformation soft finger contact problems. Int J Mech Mater Des. 2011;7(4):299–305. doi:10.1007/s10999-011-9167-1.
6. Liu Y, Jia W, Li C. A model-based study on the mechanical behaviour of hemispherical soft fingertip. Int J Comput Appl Technol. 2016;53(2):128–34. doi:10.1504/IJCAT.2016.074450.
7. Dharbaneshwer SJ, Thondiyath A. Contact area-based modeling of robotic grasps using deformable solid mechanics. Int J Appl Mech. 2021;13(3):2150038. doi:10.1142/s1758825121500381.
8. Yuvaraj S, Malayalamurthi R, Raja KV. Assessment of the contact behavior of a soft hemispherical finger tip in curved profile grasping. Int J Mater Res. 2016;107(9):777–82. doi:10.3139/146.111410.
9. Yuvaraj S, Malayalamurthi R, Gokulprasath S, Venkatesh Raja K. Assessment of contact parameters of soft splined hemispherical finger-tip pressed against a concave profile. Mater Res Express. 2018;5(6):065319. doi:10.1088/2053-1591/aac259.
10. Yuvaraj S, Malayalamurthi R, Raja KV. The haptic and perceptional characteristics of an anthropomorphic curved soft finger structure. Curved Layer Struct. 2019;6(1):161–8. doi:10.1515/cls-2019-0013.
11. Piccinini M, Berselli G, Zucchelli A, Vassura G. Predicting the compliance of soft fingertips with differentiated layer design: a numerical and experimental investigation. In: Proceedings of the 2009 International Conference on Advanced Robotics; 2009 Jun 22–26; Munich, Germany.

12. Berselli G, Vassura G. Differentiated layer design to modify the compliance of soft pads for robotic limbs. In: Proceedings of the 2009 IEEE International Conference on Robotics and Automation; 2009 May 12–17; Kobe, Japan. p. 1285–90. doi:10.1109/ROBOT.2009.5152377.
13. Kargar SM, Berselli G. Soft pads for robotic limbs: achieving human finger compliance *via* finite element optimization. Int J Adv Manuf Technol. 2024;133(11):5705–14. doi:10.1007/s00170-024-14086-6.
14. Manikanta KS, Suthapalli L, Kurre PKR, Vemuri SA, Boggarapu NR, Anantha MT. Selection of hyper-elastic materials and pattern of differentiated soft pads emulating human finger compliance in robotic fingertips. Multidiscip Model Mater Struct. 2026;22(1):218–31. doi:10.1108/mmms-04-2025-0138.
15. Tiezzi P, Vassura G. Experimental analysis of soft fingertips with internal rigid core. In: Proceedings of the ICAR'05, 12th International Conference on Advanced Robotics; 2005 Jul 18–20; Seattle, WA, USA. p. 109–14. doi:10.1109/ICAR.2005.1507399.
16. Berselli G, Piccinini M, Vassura G. On designing structured soft covers for robotic limbs with predetermined compliance. In: Proceedings of the 34th Annual Mechanisms and Robotics Conference, Parts A and B. Vol. 2; 2010 Aug 15–18; Montreal, QC, Canada. p. 165–74. doi:10.1115/detc2010-28965.
17. Raja KV, Malayalamurthi R. Assessment and influence of internal rigid core on the contact parameters for soft hemispherical fingertips. J Polym Eng. 2014;34(2):145–52. doi:10.1515/polyeng-2013-0121.
18. Raja KV, Malayalamurthi R. Assessment on the contact factors of a sandwich soft finger model—An experimental investigation. Int J Mater Res. 2015;106(5):521–6. doi:10.3139/146.111206.
19. Tiezzi P, Kao I, Vassura G. Effect of layer compliance on frictional behavior of soft robotic fingers. Adv Robot. 2007;21(14):1653–70. doi:10.1163/156855307782227390.
20. Qin L, Shi X, Wang Y, Zhou Z. Perception of static and dynamic forces with a bio-inspired tactile fingertip. J Bionic Eng. 2023;20(4):1544–54. doi:10.1007/s42235-023-00344-y.
21. Lyu B, Xiao H, Meng Q, Wu J, Wang Y, She J, et al. Humanoid finger with rigid-flexible-soft structure. Nat Commun. 2025;16(1):9905. doi:10.1038/s41467-025-65367-x.
22. Elango N, Faudzi AAM. A review article: investigations on soft materials for soft robot manipulations. Int J Adv Manuf Technol. 2015;80(5):1027–37. doi:10.1007/s00170-015-7085-3.
23. Tatara Y. Extensive theory of force-approach relations of elastic spheres in compression and in impact. J Eng Mater Technol. 1989;111(2):163–8. doi:10.1115/1.3226449.
24. Xydas N, Bhagavat M, Kao I. Study of soft-finger contact mechanics using finite elements analysis and experiments. In: Proceedings of the 2000 ICRA Millennium Conference, IEEE International Conference on Robotics and Automation, Symposia Proceedings; 2000 Apr 24–28; San Francisco, CA, USA. p. 2179–84. doi:10.1109/ROBOT.2000.846351.
25. Xydas N, Kao I. Modeling of contact mechanics and friction limit surfaces for soft fingers in robotics, with experimental results. Int J Robot Res. 1999;18(9):941–50. doi:10.1177/02783649922066673.
26. Sardo A, Tiezzi P, Vassura G. A methodological approach to design of soft fingertips for humanoid robot hands. In: Proceedings of the 2006 6th IEEE-RAS International Conference on Humanoid Robots; 2006 Dec 4–6; Genova, Italy. p. 370–5. doi:10.1109/ICHR.2006.321299.
27. Pejović-Milić A, Brito JA, Gyorffy J, Chettle DR. Ultrasound measurements of overlying soft tissue thickness at four skeletal sites suitable for *in vivo* X-ray fluorescence. Med Phys. 2002;29(11):2687–91. doi:10.1118/1.1513569.
28. Yuan XG, Zhang RJ, Zhang HW. Controllability conditions of finite oscillations of hyper-elastic cylindrical tubes composed of a class of Ogden material models. Comput Mater Contin. 2008;7(3):155–66. doi:10.3970/cmc.2008.007.155.
29. Ogden RW. Large deformation isotropic elasticity—On the correlation of theory and experiment for incompressible rubberlike solids. Proc R Soc Lond A Math Phys Sci. 1972;326(1567):565–84. doi:10.1098/rspa.1972.0026.
30. Greenwood JA. Analysis of elliptical Hertzian contacts. Tribol Int. 1997;30(3):235–7. doi:10.1016/S0301-679X(96)00051-5.
31. Johnson KL. Contact mechanics. Cambridge, UK: Cambridge University Press; 1987.

32. Xydas N, Kao I. Modeling of contact mechanics with experimental results for soft fingers. In: Proceedings of the 1998 IEEE/RSJ International Conference on Intelligent Robots and Systems. Innovations in Theory, Practice and Applications; 1998 Oct 13–17; Victoria, BC, Canada.
33. Zhu Z, Yang Z, Yang F, Yao C, Jiang H. Enhancing interfacial shear debonding resistance by mechanical mismatch. Int J Mech Sci. 2023;260(1):108656. doi:10.1016/j.ijmecsci.2023.108656.
34. Zhu Z, Yang Z, Xia Y, Jiang H. A review of debonding behavior of soft material adhesive systems. Mech Soft Mater. 2022;4(1):7. doi:10.1007/s42558-022-00045-2.
35. Shao F, Childs THC, Barnes CJ, Henson B. Finite element simulations of static and sliding contact between a human fingertip and textured surfaces. Tribol Int. 2010;43(12):2308–16. doi:10.1016/j.triboint.2010.08.003.
36. Suomalainen M, Karayiannidis Y, Kyrki V. A survey of robot manipulation in contact. Robot Auton Syst. 2022;156(3):104224. doi:10.1016/j.robot.2022.104224.
37. Kargar SM, Berselli G. Enhancing gripping stability for delicate object handling: frictional insights into textured soft pads. Int J Adv Manuf Technol. 2025;140(11–12):6413–24. doi:10.1007/s00170-025-16625-1.